

New Members of the Cluster Family in Nearby Lenticulars ¹

Jean P. Brodie and Søren S. Larsen

UC Observatories / Lick Observatory, University of California, Santa Cruz, CA 95064, USA

brodie@ucolick.org and soeren@ucolick.org

ABSTRACT

Using spectra obtained with the Keck I telescope we have demonstrated conclusively that the faint ($23 \leq V \leq 24$ mag.) and unusually extended objects we discovered in HST images of the lenticular galaxies, NGC 1023 and NGC 3384, are star clusters associated with their respective galaxies. In the case of NGC 1023 we were further able to establish that these objects are old ($\geq 7-8$ Gyr), moderately metal-rich ($[\text{Fe}/\text{H}] = -0.58 \pm 0.24$) and, having a system rotation curve which is very similar to that of the host galaxy, are associated with the lenticular disk. α -element to iron abundance ratios are highly supersolar with $[\alpha/\text{Fe}]$ between +0.3 and +0.6. With moderately high metallicities and luminosities, and effective radii in the range 7–15 pc (compared to the 2–3 pc sizes typical of normal globular and open clusters), this population of clusters has no known analog in the Milky Way or elsewhere in the Local Group.

Subject headings: galaxies: star clusters — galaxies: individual (NGC 1023, NGC 3384)

1. Introduction

During a recent search for globular clusters in the nearby (9.8 Mpc) lenticular galaxy NGC 1023 we noticed a number of objects with larger effective radii than normal globular clusters and fainter magnitudes (Larsen and Brodie 2000, hereafter Paper I). While normal globular clusters have typical effective (half-light) radii of about 3 pc and follow a roughly Gaussian magnitude distribution with a peak at $M_V \approx -7.4$ (e.g. Harris 1991), the objects in NGC 1023 were found to have larger effective radii of about 7–15 pc and were mostly *fainter* than $M_V = -7$. In Paper I we also noted that the spatial distribution of these objects seemed to indicate association with the disk of NGC 1023 and that they had predominantly red colors, indicating high metallicities and ages greater than a Gyr. At first glance, the size distributions of these objects are reminiscent of the few faint “Palomar” type globular clusters in the outer halo of the Milky Way. However, as we shall show, the spatial

¹Based on data obtained at the W. M. Keck Observatory, which is operated as a scientific partnership among the California Institute of Technology, the University of California and the National Aeronautics and Space Administration.

and luminosity distributions as well as kinematics and metallicities of the much more numerous faint extended objects in NGC 1023 are strikingly different, defining a new parameter space which must be accommodated in cluster formation models.

Because of the faintness of these clusters, it is not surprising that they have not been noticed before in the numerous HST-based studies of extragalactic globular clusters. With M_V magnitudes fainter than -7 , they will generally have apparent magnitudes fainter than $V = 24$ even at the distance of the Virgo or Fornax clusters, and are thus easily missed or discarded as possible background galaxies. Furthermore, size information is necessary to recognize them as different from normal globular clusters. In Larsen et al. (2001), a smaller number of faint, extended objects similar to those in NGC 1023 were noted in another nearby (11.5 Mpc, Sakai et al. 1997) lenticular, NGC 3384, but their existence was ruled out in two other nearby early-type galaxies, NGC 3115 (a lenticular) and NGC 3379 (an elliptical).

In this paper we show that the faint extended objects in NGC 1023 and NGC 3384 occupy a new region of the size/luminosity/metallicity parameter space for star clusters. We present new Keck / LRIS spectra of these clusters to verify membership with NGC 1023 and NGC 3384 and disprove the (albeit unlikely) possibility that the objects are unrelated background galaxies. We also measure radial velocities for individual objects and examine the hypothesis that they are associated with the disk, in which case strong signatures of rotation around the center of the galaxy should be seen. We then use the co-added spectra of all objects to put constraints on their ages and metallicities. We end with a discussion of the factors which may have influenced the formation and survival of these clusters.

2. Data

The cluster candidates were selected from the WFPC2 data of Paper I, where all aspects of the photometry and measurement of object sizes have been discussed. Figure 1 illustrates the selection criteria: The lower panels are color-magnitude diagrams with symbol size proportional to the object sizes, while the upper panels show object size vs. $V-I$ color for objects brighter than $V = 24$. The faint extended objects are easily identifiable in the color-magnitude diagrams, with $V-I \approx 1.3$ and with FWHM values between 1 and 2 pixels, corresponding to effective radii of 7 – 15 pc. The boxes indicate the selection criteria for objects to be included in the Keck / LRIS slitmasks.

Although relative positions of objects measured on a single WFPC2 image would easily be accurate enough to provide coordinates for slitmask design, significant offsets ($1-2''$) can be present between individual WFPC2 pointings. Since the objects in NGC 1023 were selected from two WFPC2 pointings, we therefore re-identified the clusters on an image of NGC 1023 taken with LRIS during an earlier observing run and used positions measured on the LRIS image to provide the final coordinate lists. For NGC 3384, only one WFPC2 pointing was used for object selection

and the coordinates measured on the WFPC2 image were used directly for the slitmask design.

The observations were carried out on Dec 9 and Dec 10, 2001 in multi-slit mode with the LRIS spectrograph (Oke et al. 1995) on the Keck I telescope. Spectra were obtained simultaneously with the two arms on LRIS, using a dichroic that split at a wavelength of ~ 5600 Å. On the blue side a 400 l/mm grism was used, providing a spectral resolution of about 8 Å in the range ≈ 3500 – 5500 Å. On the red side we used a 400 l/mm grating blazed at 7500 Å, covering the range ~ 5700 – 9000 Å with a similar resolution. We had intended to use the red spectra, and the Ca II triplet at ~ 8500 – 8700 Å in particular, to determine radial velocities, but the strong atmospheric OH bands made it impossible to extract useful spectra for these very faint objects at wavelengths $\gtrsim 8000$ Å. However, for some objects we could measure radial velocities using the wavelength region ~ 5700 – 7000 Å on the red spectra. The total integration times for NGC 1023 and NGC 3384 were 570 min (9 hours 30 min) and 300 min (5 hours), respectively, divided into 1 hour integrations.

Spectral reductions were carried out using the SPECRED package in IRAF². Wavelength calibrations were performed using spectra of calibration lamps mounted within LRIS, taken immediately after the last exposure of each galaxy. For the blue side, comparison with calibration spectra taken during the afternoon showed shifts of about 3–4 Å, probably due to flexure in the instrument. For the red spectra the wavelength zero-points were corrected using the OI line at 6300.304 Å, in some cases by up to ~ 5 Å. No skylines are included in the blue spectra, making it difficult to test whether shifts in the zero-point of the wavelength scale are present between the individual exposures, and the spectra extracted from individual exposures were too faint to test for such differences by cross-correlation. However, we extracted spectra of the underlying galaxy light and cross-correlated these to test for any shifts in the wavelength scale, and found no systematic differences between individual exposures larger than 1 Å.

Data for the observed cluster candidates in NGC 1023 and NGC 3384 are listed in Tables 1 and 2. Radial velocities were measured by cross-correlating the object spectra with spectra of three stars of spectral types G0–K3 (numbers 17495, 33815 and 36094 in the recent compilation by Barbier-Brossat & Figon 2000). The cross-correlation was done with the FXCOR task in the RV task in IRAF. Whenever possible, we measured radial velocities on both the blue and red spectra. The tables list all candidate clusters included in the LRIS slitmasks, including a few for which no significant cross-correlation peak was found. Some of these have very poor S/N, and for others the delicate extraction of the faint spectra was compromised because of internal reflections (“ghosts”) in the blue arm of the spectrograph or uncertain background subtraction because the object was located near the end of a slitlet. It can, of course, not be ruled out that some of these objects are indeed background galaxies and that this is the reason why no cross-correlation signal was found anywhere near the expected radial velocity. However, it is clear that the vast majority of the objects have radial velocities indicating association with NGC 1023 or NGC 3384.

²IRAF is distributed by the National Optical Astronomical Observatories, which are operated by the Association of Universities for Research in Astronomy

The unweighted means of the cluster velocities for NGC 1023 and NGC 3384, measured on the blue spectra, are 692 ± 56 km/s and 1149 ± 43 km/s respectively, in both cases larger than the RC3 values for NGC 1023 (601 km/s) and NGC 3384 (704 km/s). However, for the clusters with radial velocity measurements on both blue and red spectra, the mean differences are $\langle V_b - V_r \rangle = 133 \pm 31$ km/s for NGC 1023 and $\langle V_b - V_r \rangle = 381 \pm 54$ km/s for NGC 3384. If all the radial velocities measured on the blue spectra are corrected for these differences then the mean values become 559 ± 64 km/s and 768 ± 79 km/s, respectively, in much better agreement with the cataloged values for the parent galaxies.

3. The characteristics of the faint extended clusters

3.1. Uniqueness

Are these objects really something new? After all, it is well known that the Milky Way hosts several diffuse faint clusters and there is at least one (NGC 2257) in the LMC (Elson & Freeman 1985). In Fig. 2 we show the absolute magnitudes of Milky Way globular clusters as a function of their metallicities, where the data are from Harris (1996). We used $[\text{Fe}/\text{H}]$ rather than color here because metallicity is available for more clusters than $V - I$ or any other color. As in the lower panels of Fig. 1, the sizes of the points in this plot correspond to the half-light radii of the clusters. The box in this figure corresponds to the selection box in the lower left panel of Fig. 1. Clearly, there are no Milky Way objects which correspond in metallicity (color), luminosity and size to the faint extended clusters in NGC 1023. There are a few Milky Way objects which have similar sizes and luminosities but their metallicities are extremely different. This is true too of the extended cluster in the LMC. The group of “Palomar-Like” Milky Way globular clusters are clearly present as a small group of lower-luminosity blue objects. Such objects might also be present in NGC 1023 but would be below the limit where we can reliably measure sizes.

NGC 1023 has 29 objects with half-light radii, R_h , greater than 7 pc and $V < 24$ (i.e. M_V brighter than -6.2 , our limit for secure size measurement). According to Harris (1996), the Milky Way has 19 globular clusters larger than 7 pc but only 6 of these are brighter than $M_V = -6.2$. All clusters with $R_h > 7$ pc in the Milky Way are located more than 4 kpc from the plane of the Galactic disk and all but one are located at 20–80 kpc from the center of the Galaxy (the remaining one is at 7 kpc from the center). The extended clusters in the Milky Way are clearly not associated with its disk but are rather outer halo objects, presumably formed in the low density environment in the outskirts of the protogalaxy (McLaughlin 2000).

We note in passing that Milky Way open clusters, contrary to common misconception, are not particularly large, except for those which are extremely young (≤ 10 Myr) and presumably unbound. Milky Way open clusters are, in any case, significantly less massive than the faint extended clusters in NGC 1023 (Janes et al. 1988).

3.2. System Rotation

From their mean velocities it is clear that the faint extended clusters are associated with their respective galaxies and do not constitute a background population. Moreover, in Fig. 3, the radial velocity plot for the faint extended clusters in NGC 1023, we see clear evidence for rotation of the cluster system and this kinematic signature corresponds quite closely to the rotation of the galaxy itself, as measured along the major axis by Simien & Prugniel (1997). The cluster radial velocities were measured from the blue spectra and have been corrected by -133 km/s as determined in Section 2. The bulge effective radius for NGC 1023 is <2 kpc (Möllenhoff & Heidt 2001) so the clusters are ~ 2 bulge effective radii from the galaxy center ($1' = 2.9$ kpc at the distance of NGC 1023). This strongly suggests that these objects are associated with the galaxy’s disk rather than its bulge.

In Fig. 4 we show, for comparison, the radial velocities of the compact globular clusters in NGC 1023, taken from Larsen & Brodie (2002). Although the sample is small, there is no hint of rotation in the compact cluster system.

Although there are too few clusters to provide any dynamical constraints on the NGC 3384 extended cluster system, in Fig. 5 we show, for completeness, the radial velocities of the extended clusters and the NGC 3384 rotation curve from Fisher (1997).

3.3. Ages and Metallicities

The spectra of these extended objects are very similar to those of moderately metal-rich old globular clusters. Metallicities were determined from a weighted combination of line strength indices according to the prescription of Brodie and Huchra (1990). Because of the low S/N of the individual spectra, a “master” spectrum (blue: Fig. 6, red: Fig. 7) was produced by co-adding all spectra with known radial velocities, shifted to 0 velocity. For 14 clusters in NGC 1023, each with an exposure time of 9.5 hours, the “master” spectrum represents a total of 133 hours of 10-meter telescope time. This co-added spectrum has a S/N of 17 per pixel (i.e. ~ 34 per resolution element) and yields a mean $[\text{Fe}/\text{H}] = -0.58 \pm 0.24$. The average reddening-corrected $V - I$ color ($\langle V - I \rangle_o = 1.22$) corresponds to $[\text{Fe}/\text{H}] = -0.51$, using the color-metallicity conversion relation of Kissler-Patig et al. (1998), in excellent agreement with the spectroscopic value. Index values and metallicities derived from the “master” spectrum are given in table 3.

Values of $[\text{Fe}/\text{H}]$ and $\text{H}\beta$ measured on the NGC 1023 “master” spectrum were compared to Maraston & Thomas (2000) stellar evolutionary models (Fig 8). This yields only loose constraints on cluster ages which are most probably ~ 13 Gyr old, but ages as young as $\sim 7-8$ Gyr are not ruled out. The lower limit on $\text{H}\beta$ is well below any model predictions so our data do not put any constraints on the upper age limit of the clusters.

The fact that these objects are old suggests that they are quite stable against disruption. It

might indicate that they are on roughly circular orbits as this would be likely to minimize disruptive effects (disk/bulge shocking, etc).

A similar summation exercise for NGC 3384, excluding N3384-FF-7, which is over a magnitude brighter than the other extended clusters and which may be a “normal” (but large) globular cluster, produces a co-added spectrum with $S/N = 9$ per pixel. For these 5 clusters, each with 5 hours of integration, the equivalent exposure time of the co-added spectrum is 25 hours. It yields a mean $[Fe/H]$ estimate of -1.13 ± 0.45 . The average reddening-corrected $V - I$ color ($\langle V - I \rangle_o = 1.27$) corresponds to $[Fe/H] = -0.35$, using the Kissler-Patig et al. (1998) relation. If N3384-FF-7 is included, the S/N increases to 11 and $[Fe/H] = -0.64 \pm 0.34$. The mean color is unchanged. Because of the large errors on $[Fe/H]$ and $H\beta$, no useful constraints on age can be obtained even from the summed spectrum. Table 4 gives the relevant indices from the NGC 3384 “master” spectrum. $TiO_{12.5}$ is not included because a red summed spectrum was not formed for this galaxy due to poor signal-to-noise.

3.4. α -element to iron ratios

Relations between Mgb and $[Fe/H]$ (Fig 9) and $TiO_{12.5}$ and $[Fe/H]$ (Fig 10) for various levels of α -element enhancement were produced from the SSP models of Milone et al. (2000), assuming a Salpeter IMF. For comparison with our cluster measurements, the $Mg2$ values provided in Milone et al. (2000) were converted to Mgb using the relation $Mgb = 14.03 \times Mg2 + 0.361$, derived from the Maraston models as in Larsen et al. (2002). This conversion is accurate to $\leq 0.1\text{\AA}$ for ages between 10 and 15 Gyr. $[Fe/H]$ is used rather than $\langle Fe \rangle$ because the latter is an average of two Fe indices Fe5270 and Fe5335, the redder of which is close to the edge of our spectral range and is poorly determined in our data. We note, however, that since Mg is a component in the $[Fe/H]$ determination, if the objects are α -enhanced, the resultant $[Fe/H]$ value will be too high. Data points from the NGC 1023 “master” spectrum indicate that the $[\alpha/Fe]$ ratio for the faint extended objects is between +0.3 and +0.6. Any adjustment for the inflated $[Fe/H]$ values will move points to the left in the plots and will tend to further increase the α -enhancement. Also shown in Fig 9 is the relation from Maraston (2001) for a 12 Gyr SSP model. Since many of the metal-poor stars used in deriving the Maraston relation may be α -enhanced (Maraston & Thomas 2000), its agreement with the Milone et al. (2000) α -enhanced curves is not surprising. $[\alpha/Fe]$ ratios of $\sim +0.3$ are typical for old stellar populations in the bulge and halo of the Milky Way (Carney 1996) and the globular clusters and starlight of elliptical galaxies (Forbes et al. 2001; Milone et al. 2000) and are interpreted as indicating rapid, early chemical element enrichment dominated by Type II supernovae.

4. Discussion

Observational evidence (Larsen et al. 2001; Burgarella, Kissler-Patig & Buat 2001; Kundu & Whitmore 2001) and current ideas about the origins of globular cluster sub-populations (Ashman & Zepf 1992; Forbes Brodie & Grillmair; van den Bergh 2001) suggest that the origins of *compact* red (metal-rich) and blue (metal-poor) globular clusters may have been quite different, occurring at different epochs or under different physical mechanisms, or both.

A striking difference between the blue and red subpopulations of compact globular clusters, which is especially interesting in regard to these faint extended red clusters, is that within the “normal” compact globular cluster population, the red globulars are always $\sim 25\%$ *smaller* than their blue counterparts (Larsen et al. 2001; Kundu & Whitmore 1998; Puzia et al. 1999). These considerations underscore the fundamentally different nature of the population of red extended objects in these lenticular galaxies.

Perhaps clues about the origins of these objects can be found by asking what NGC 1023 and NGC 3384 have in common that differentiates them from NGC 3115. NGC 1023 is the dominant member of a well-defined group of 15 galaxies and NGC 3384 is a member of the Leo I group (Garcia 1993). By contrast, NGC 3115 is isolated except for a dwarf companion NGC 3115DW at a distance of 5.5 arcmin (~ 17.5 kpc). Both NGC 1023 and NGC 3384 are classified as SB0s while NGC 3115 is a highly bulge-dominated galaxy, transitional in type between E7 and S01. In Paper I we speculated that the faint extended cluster population in NGC 1023 might have originated in encounters with dwarf companion galaxies. According to Harris & Pudritz (1994), massive cluster formation occurs within supergiant molecular clouds that are pressure-confined by the parent galaxy’s interstellar medium. Therefore, more extended clusters would naturally form in lower-density environments like the outer regions of giant galaxies and the weak potential wells of dwarf galaxies. Similarly, McLaughlin (2000) has noted a relation between cluster binding energy and galactocentric radius for Milky Way globular clusters which implies extended cluster formation in low ambient density environments. These considerations might lend support to the idea that the faint extended clusters formed in dwarfs before joining NGC 1023. Young star clusters have formed recently in the nearby dwarf, NGC 1023A (Larsen & Brodie 2002) but with no HST observations of this companion galaxy, we cannot say whether these new clusters are extended. It would be natural to suppose that more dwarf companion galaxies were present in the past in the vicinity of NGC 1023 and NGC 3384, given their presence in significant groups.

Alternatively, the fact that NGC 3115 has such a modest disk may be the relevant feature. It is difficult to preferentially destroy compact objects while preserving extended ones so, if the faint extended clusters formed in the disk, the ambient conditions (gas densities?) there may have been conducive to forming only extended objects. Lenticulars with well-developed disks may provide an environment for the formation of star clusters with unique characteristics.

Another factor may be the sizes of the black holes at the centers of these galaxies. NGC 3115 has a much more massive ($9.1 \times 10^8 M_\odot$) black hole in its center than do NGC 1023 ($3.9 \times 10^7 M_\odot$)

and NGC 3384 ($1.8 \times 10^7 M_{\odot}$), where the black hole masses are from Ho (2002). In other words old clusters in NGC 3115 may have been subjected to quasar-like environmental conditions during their youth, whereas clusters in NGC 1023 and NGC 3384 might have spent their youths in less stressful environments (van den Bergh 2002).

5. Conclusions

We have demonstrated conclusively that the faint extended objects discovered in HST images of NGC 1023 and NGC 3384 are star clusters associated with their respective galaxies. In the case of NGC 1023 we were further able to establish that these objects are old, moderately metal-rich and, having a system rotation which is very similar to the rotation curve of the host galaxy, are associated with the lenticular disk.

As a population, these star clusters have no known analog in the Milky Way or indeed elsewhere in the Local Group. Comparisons with the Milky Way “Palomar-like” extended clusters confirms that the Milky Way objects are similar only in size. They differ in number, kinematics, location with respect to the disk and the Galaxy center, metallicity and luminosity. In short, the Milky Way objects are a small halo population of metal-poor, low-luminosity clusters while the NGC 1023 cluster are numerous, metal-rich, disk objects which rotate as an ensemble.

These new members of the cluster family have been discovered in two lenticular galaxies and the presence of similar objects has been definitely ruled out in a third lenticular as well as in a nearby elliptical galaxy. Existing HST data for other galaxies are inadequate to establish either the presence or the absence of such clusters so, without further observations, we cannot ascertain how common this phenomenon might be and whether or not these newly-discovered objects are found exclusively in lenticular galaxies. If so, they are not found in *all* lenticulars. Late-type S0s may offer a more suitable environment for the formation of extended clusters than early-type lenticulars. The size of the host galaxy’s central black hole may be a governing factor in allowing an appropriate environment for the survival of extended disk clusters. If galaxy-galaxy interactions play a role in forming these clusters, group (or galaxy cluster) membership may be a relevant criterion for selecting host galaxy candidates.

We thank Sidney van den Bergh, Duncan Forbes and an anonymous referee for helpful comments and suggestions. This work was supported by National Science Foundation grant number AST-9900732.

REFERENCES

Ashman, K. M. and Zepf, S. E., 1992 ApJ, 429, 557

- Barbier-Brossat M. & Figon P. 2000, A&AS, 142, 217 A&AS, 106, 275
- Brodie, J. P. and Huchra, J. P. 1990, AJ, 362, 503
- Burgarella, D., Kissler-Patig, M., and Buat, V., 2001, AJ, 121, 2647
- Carney, B. 1996, PASP, 108, 900
- Elson, R. A. W. and Freeman, K. C., 1985, ApJ, 288, 521
- Fisher, D. 1997, AJ, 113, 950
- Forbes, D. A., Brodie, J. P., and Grillmair, C., 1997, AJ, 113, 1652
- Forbes, D. A., Beasley, M. A., Brodie, J. P., & Kissler-Patig, M. 2001, ApJL 563, 143
- Garcia, A. M. 1993, A&AS, 100, 47
- Harris, W. E. 1991, ARAA, 29, 543
- Harris, W. E. 1996, AJ112, 1487
- Harris, W. E., and Pudritz, R. E. 1994, ApJ, 429, 177
- Ho, L., 2002, ApJ564, 120
- Janes, K. A., Tilley, C., and Lyngå, G., 1988, AJ, 95, 771
- Kissler-Patig, M., Brodie, J. P., Schroder, L. et al., 1998, AJ, 115, 105
- Kundu, A. and Whitmore, B., 1998, AJ, 116, 2841
- Kundu, A. and Whitmore, B., 2001, AJ, 121, 2950
- Larsen, S. S., and Brodie, J. P., 2000, AJ, 120, 2938 (Paper I)
- Larsen, S. S., Brodie, J. P., Huchra, J. P., Forbes, D. A. and Grillmair, C. 2001, AJ, 121, 2974
- Larsen, S. S., and Brodie, J. P., 2002, AJ, in press
- Larsen, S. S., Brodie, J. P., Beasley, M., and Forbes, D. A., 2002, AJ, submitted
- Maraston, C., 2001, Private communication
- Maraston, C. & Thomas, D. 2000, ApJ, 541, 126
- McLaughlin, D. E. 2000, ApJ, 539, 618
- Milone, A., Barbay, B., & Schiavon, R. P. 2000, AJ, 120, 131
- Möllenhoff, C., & Heidt, J., 2001, A&AS, 268, 16

- Oke, J. B. Cohen, J. G., Carr, M. et al. 1995, PASP, 107, 375
- Puzia, T. H., Kissler-Patig, M., Brodie, J. P., and Huchra, J. P., 1999, AJ118, 2734
- Sakai, S., Madore, B. F., and Freedman, W. L., 1997, ApJ, 478, 49
- Simien, F. & Prugniel, P. 1997, A&AS, 126, 519
- van den Bergh, S. 2001, ApJL, 559, 113
- van den Bergh, S. 2002, private communication
- Worthey, G., Faber, S. M., González, J. J., and Burstein, D. 1994,

Table 1. Spectroscopic data for cluster candidates in NGC 1023

Object	RA(2000)	DEC(2000)	V	$V-I$	RV (km/s)		S/N
					blue	red	
NGC 1023	2:40:24.1	39:03:46	-	-	601		-
N1023-FF-1	2:40:34.73	39:02:58.6	23.60 ± 0.03	1.19 ± 0.04	1011 ± 48	-	3.6
N1023-FF-2	2:40:33.79	39:04:31.2	23.29 ± 0.02	1.39 ± 0.03	994 ± 9	-	5.0
N1023-FF-3	2:40:32.79	39:04:10.8	23.62 ± 0.03	1.39 ± 0.03	-	-	2.1
N1023-FF-4	2:40:31.94	39:03:42.9	23.82 ± 0.03	1.20 ± 0.04	736 ± 40	-	2.2
N1023-FF-5	2:40:29.96	39:03:36.3	22.56 ± 0.01	1.27 ± 0.02	1015 ± 35	888 ± 6	8.6
N1023-FF-6	2:40:29.34	39:03:17.2	23.65 ± 0.03	1.33 ± 0.04	811 ± 78	663 ± 21	3.9
N1023-FF-7	2:40:28.78	39:03:17.9	23.46 ± 0.02	1.36 ± 0.03	666 ± 73	565 ± 4	4.5
N1023-FF-8	2:40:28.20	39:03:47.1	23.68 ± 0.03	1.39 ± 0.03	-	-	2.6
N1023-FF-9	2:40:27.50	39:04:15.7	23.40 ± 0.02	1.28 ± 0.03	648 ± 98	-	3.5
N1023-FF-10	2:40:26.40	39:04:19.6	23.31 ± 0.02	1.31 ± 0.03	614 ± 78	629 ± 66	6.6
N1023-FF-11	2:40:23.53	39:04:24.4	23.71 ± 0.03	1.36 ± 0.04	-	-	-
N1023-FF-12	2:40:21.55	39:04:16.6	22.99 ± 0.02	1.30 ± 0.02	514 ± 8	394 ± 17	6.9
N1023-FF-13	2:40:20.02	39:02:55.1	23.79 ± 0.03	1.18 ± 0.04	571 ± 30	-	2.5
N1023-FF-14	2:40:19.58	39:04:36.7	23.23 ± 0.02	1.34 ± 0.03	725 ± 17	489 ± 45	7.7
N1023-FF-15	2:40:18.62	39:02:55.7	23.56 ± 0.02	1.40 ± 0.03	588 ± 31	322 ± 6	4.0
N1023-FF-16	2:40:17.72	39:02:52.3	23.29 ± 0.02	1.01 ± 0.03	351 ± 25	-	6.5
N1023-FF-17	2:40:16.92	39:04:04.2	23.16 ± 0.02	1.22 ± 0.03	-	-	6.5
N1023-FF-18	2:40:16.35	39:03:29.0	22.68 ± 0.01	1.28 ± 0.02	438 ± 38	355 ± 12	7.0
N1023-FF-19	2:40:15.66	39:03:48.1	23.49 ± 0.02	1.37 ± 0.03	-	-	-

Note. — FF = “Faint Fuzzies” our informal name for the faint extended clusters, RV = heliocentric radial velocity, V = visual magnitude. The S/N column gives the average signal-to-noise per pixel on the blue spectra in the region 4000Å– 5000 Å. The photometry has not been corrected for reddening.

Table 2. Spectroscopic data for cluster candidates in NGC 3384

Object	RA(2000)	DEC(2000)	V	$V-I$	RV (km/s)		S/N
					blue	red	
NGC 3384	10:48:17.2	12:37:49	-	-	704		-
N3384-FF-1	10:48:17.50	12:38:29.7	23.28 ± 0.09	1.15 ± 0.12	-	-	4.7
N3384-FF-2	10:48:16.39	12:37:01.4	23.66 ± 0.12	1.35 ± 0.14	-	-	1.4
N3384-FF-3	10:48:15.23	12:36:45.2	22.75 ± 0.06	1.30 ± 0.06	1100 ± 49	609 ± 48	3.9
N3384-FF-4	10:48:15.00	12:39:10.9	23.60 ± 0.12	1.24 ± 0.17	1299 ± 21	-	9.9
N3384-FF-5	10:48:14.80	12:39:02.4	23.68 ± 0.13	1.29 ± 0.15	-	-	2.8
N3384-FF-6	10:48:14.16	12:37:34.2	22.87 ± 0.06	1.36 ± 0.07	1011 ± 15	-	4.8
N3384-FF-7	10:48:13.99	12:37:14.3	21.51 ± 0.02	1.26 ± 0.03	1151 ± 3	905 ± 23	15.8
N3384-FF-8	10:48:13.73	12:38:29.3	23.81 ± 0.14	1.25 ± 0.17	-	-	1.2
N3384-FF-9	10:48:12.72	12:36:29.3	23.29 ± 0.09	1.24 ± 0.11	1094 ± 42	654 ± 27	6.5
N3384-FF-10	10:48:12.33	12:36:45.3	23.32 ± 0.09	1.19 ± 0.11	1242 ± 24	895 ± 30	1.9
N3384-FF-11	10:48:10.46	12:38:29.7	23.60 ± 0.12	1.34 ± 0.14	-	-	2.8

Note. — FF = “Faint Fuzzies”, our informal name for the faint extended clusters, RV = heliocentric radial velocity, V = visual magnitude. The S/N column gives the average Signal-to-Noise per pixel in the region 4000Å– 5000 Å.

Table 3. Indices measured from the NGC 1023 summed spectrum

Index	Mag./Å	[Fe/H]	Ref.
Delta	0.627±0.019	-0.44±0.37	1
Mg2	0.215±0.013	-0.07±0.36	1
MgH	0.111±0.010	0.45±0.52	1
Gband	0.126±0.028	-1.02±0.44	1
CNB	0.101±0.029	-1.27±0.38	1
Fe5270	0.073±0.010	-0.60±0.64	1
CNR	0.070±0.020	-0.68±0.47	1
HK	0.301±0.029	-0.83±0.48	1
Hβ	1.868±0.477		2
Mgb	3.277±0.322		2
TiO _{12.5}	22.340±4.637		3

Note. — References: (1) Brodie and Huchra (1990), (2) Worthey et al. (1994), (3) Milone et al. (2000). Brodie & Huchra indices are measured in magnitudes, the rest are equivalent widths in Å. The [Fe/H] values are metallicities derived from each individual index strength. The final quoted metallicity is a weighted mean of the individual index measurements as in Brodie and Huchra (1990).

Table 4. Indices measured from the NGC 3384 summed spectrum

Index	Mag./Å	[Fe/H]	Ref.
Delta	0.640±0.026	-0.39±0.37	1
Mg2	0.137±0.025	-0.82±0.42	1
MgH	0.085±0.021	-0.04±0.64	1
Gband	-0.017±0.048	-2.65±0.63	1
CNB	0.312±0.078	0.11±0.61	1
Fe5270	0.040±0.027	-1.27±0.82	1
CNR	-0.064±0.041	-1.66±0.54	1
HK	0.181±0.063	-1.79±0.66	1
Hβ	1.308±1.13		2
Mgb	1.191±0.954		2

Note. — References: (1) Brodie and Huchra (1990), (2) Worthey et al. (1994). Brodie & Huchra indices are measured in magnitudes, Worthey indices are equivalent widths in Å. The summed spectrum does not include N3384-FF-7. TiO_{12.5} is not given for NGC 3384 because the signal-to-noise did not warrant producing a red summed spectrum. The [Fe/H] values are metallicities derived from each individual index strength. The final quoted metallicity is a weighted mean of the individual index measurements as in Brodie and Huchra (1990).

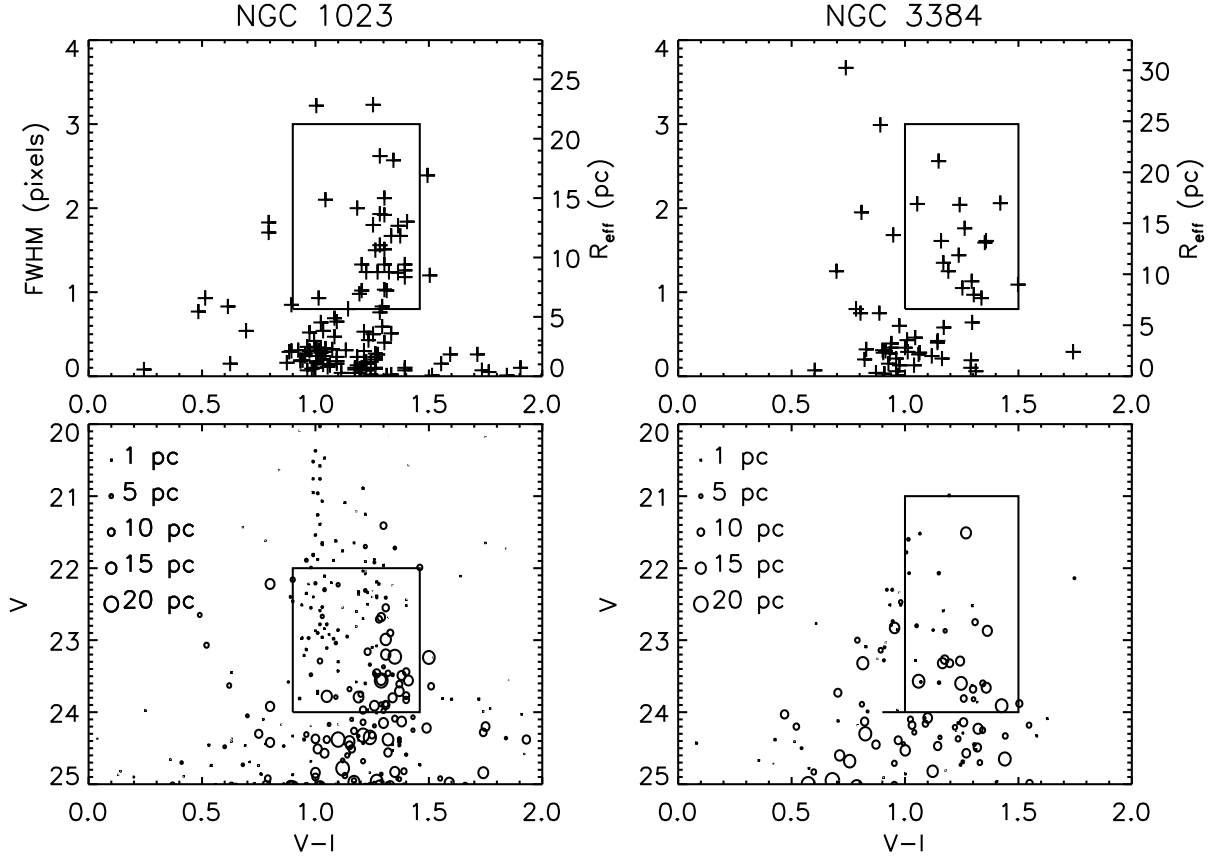


Fig. 1.— Selection of cluster candidates for spectroscopy. The lower panels are color-magnitude diagrams with symbol sizes proportional to the object sizes. The upper panels show object size vs. $V-I$ color for objects brighter than $V = 24$. The boxes indicate the selection criteria for objects to be included in the Keck / LRIS slitmasks.

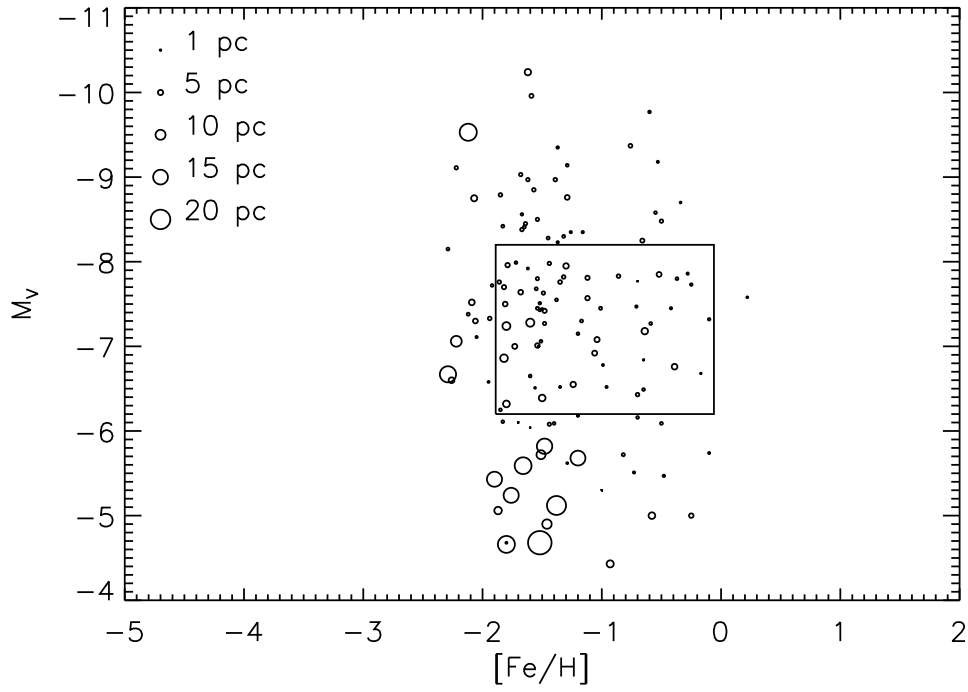


Fig. 2.— Absolute V magnitude vs. $[Fe/H]$ for Milky Way globular clusters. The symbol sizes are proportional to the object sizes. The box corresponds to the selection box in the lower left panel of Figure 1.

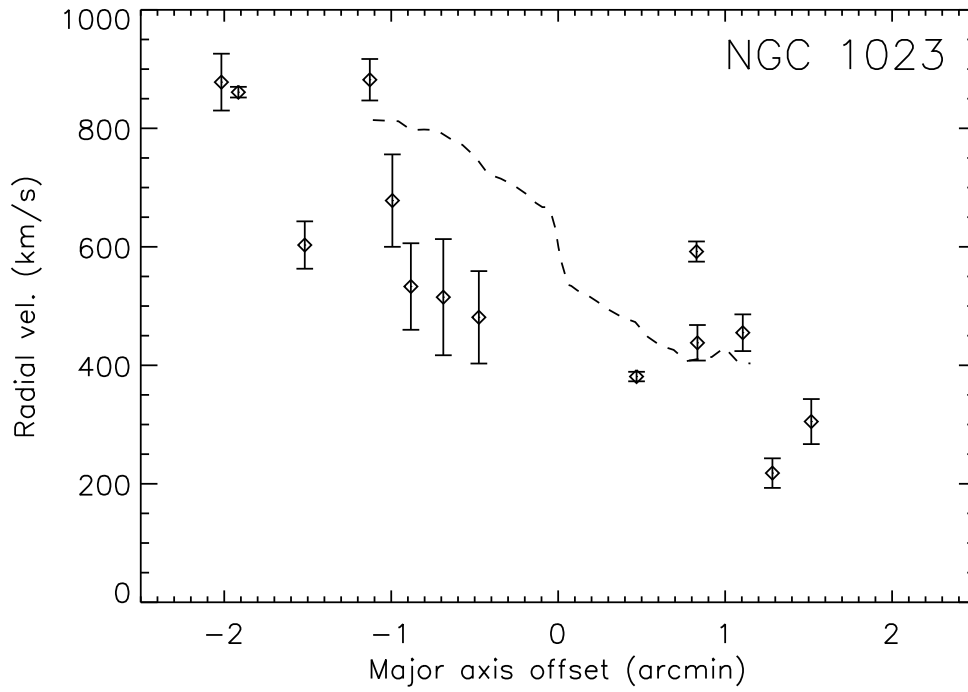


Fig. 3.— Radial velocity vs. projected distance from the galaxy center along the major axis for extended clusters in NGC 1023. The radial velocities were measured from the blue spectra, applying a correction of -133 km/s (see text). The dashed line indicates the rotation curve for NGC 1023 itself from a longslit positioned along the major axis, from Simien & Prugniel (1997).

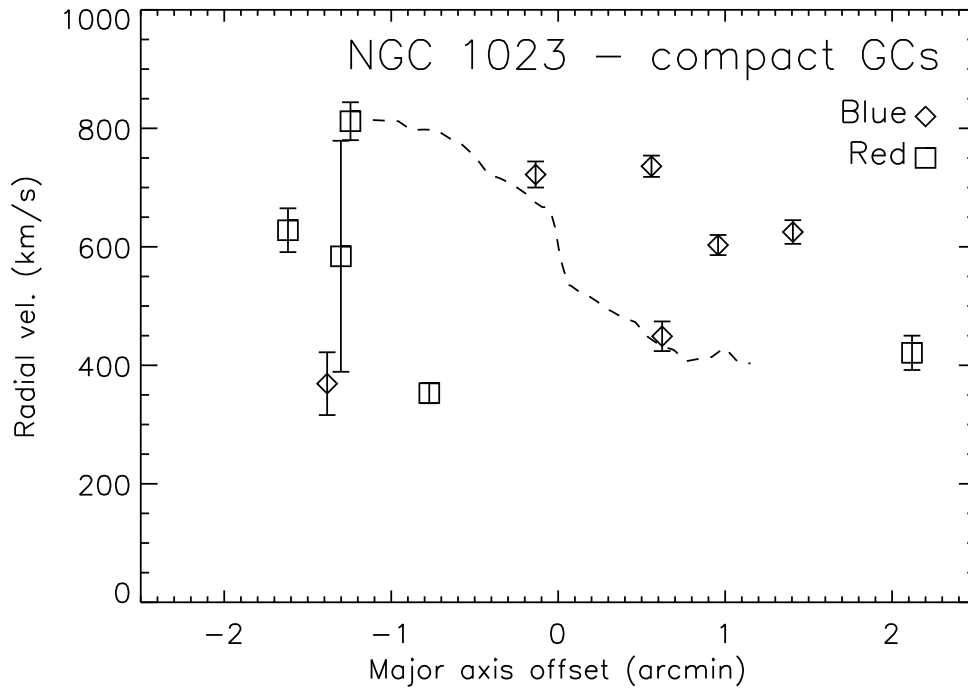


Fig. 4.— Radial velocity vs. projected distance from the galaxy center along the major axis for compact (globular) clusters in NGC 1023 from data in Larsen & Brodie (2002). The dashed line is the galaxy rotation curve as in Figure 3.

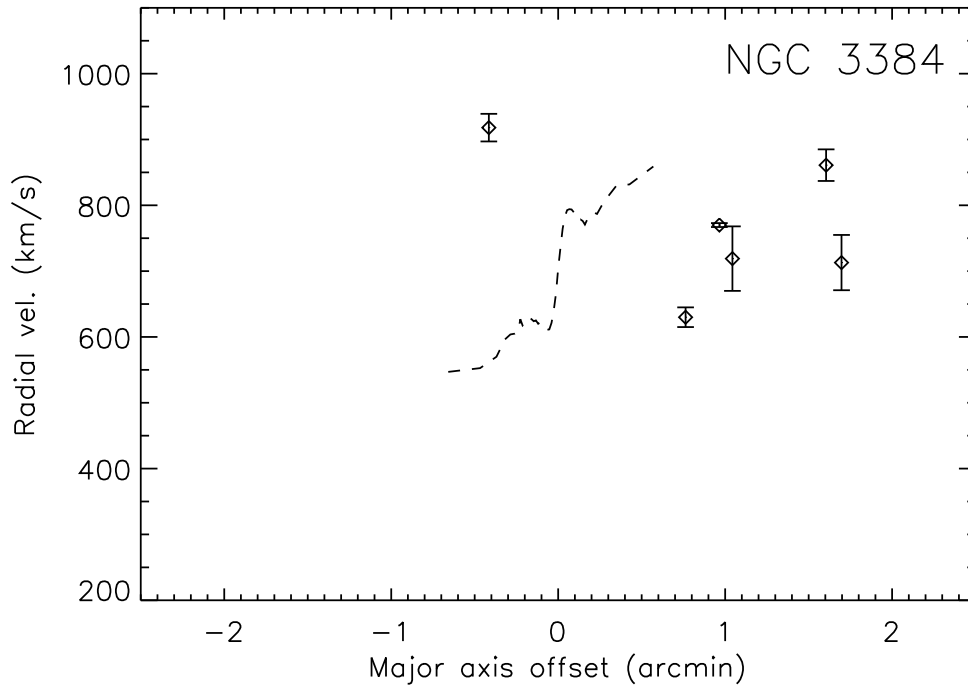


Fig. 5.— Radial velocity vs. projected distance from the galaxy center along the major axis for cluster candidates in NGC 3384. Overplotted is the rotation curve for NGC 3384 from Fisher (1997).

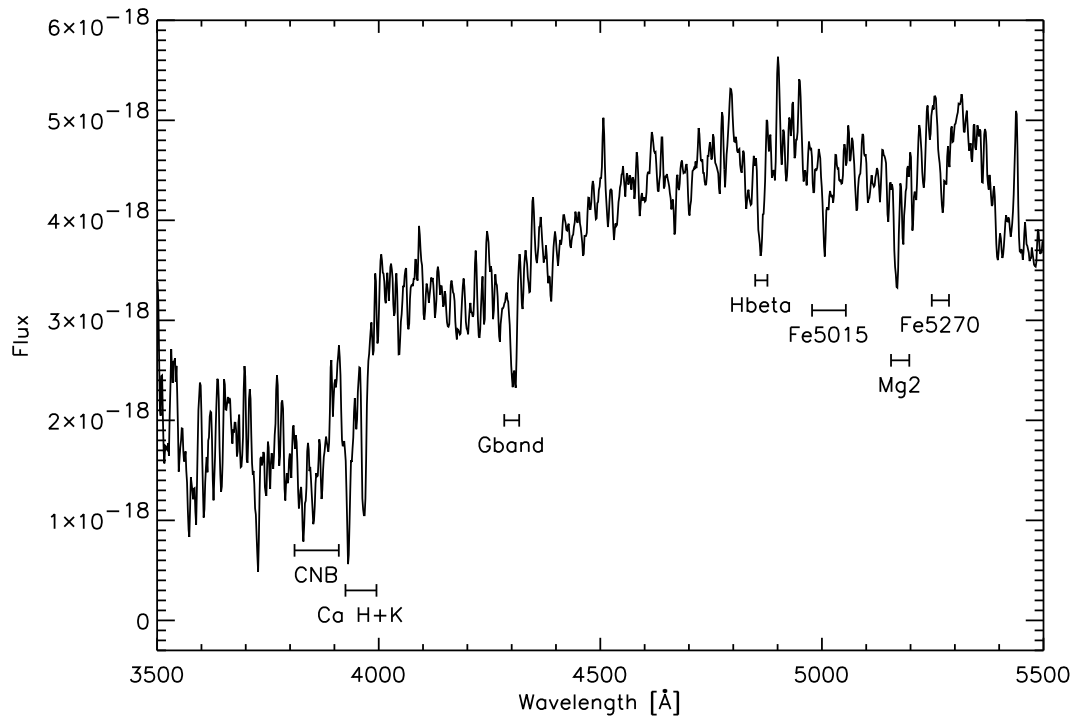


Fig. 6.— Co-added blue spectrum of all clusters in NGC 1023 with known radial velocities. The spectrum has been smoothed with a 3 pixels boxcar filter. Various spectral features are indicated.

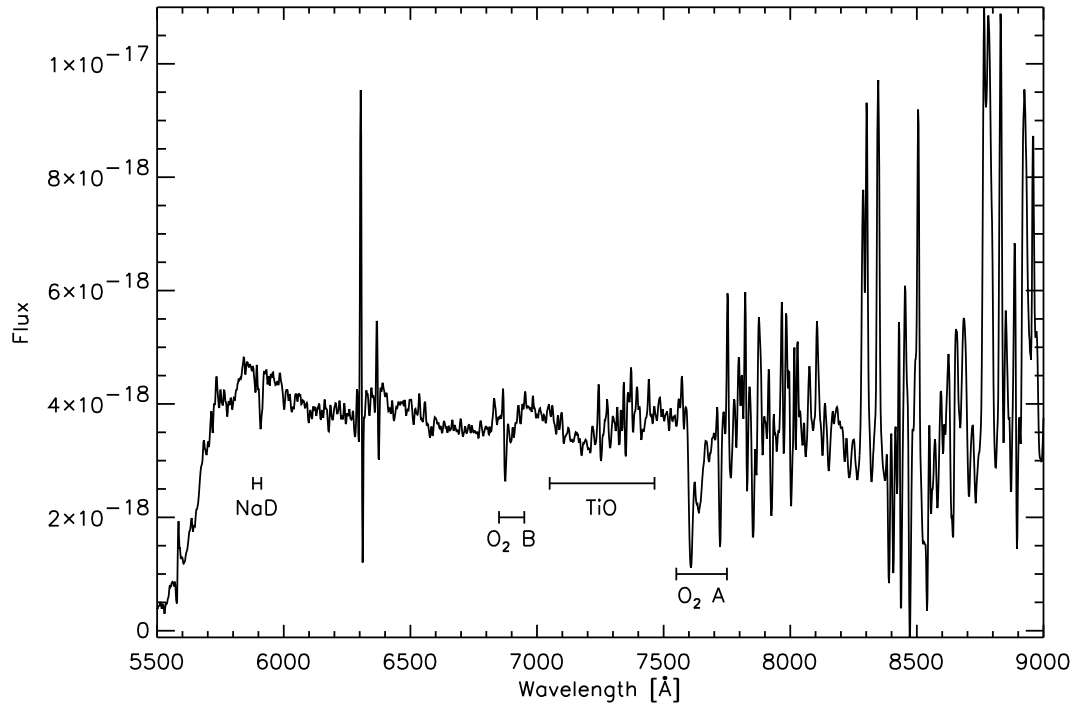


Fig. 7.— Co-added red spectrum of all clusters in NGC 1023 with known radial velocities. The spectrum has been smoothed with a 3 pixels boxcar filter. Various spectral features are indicated, including the terrestrial O₂ absorption bands.

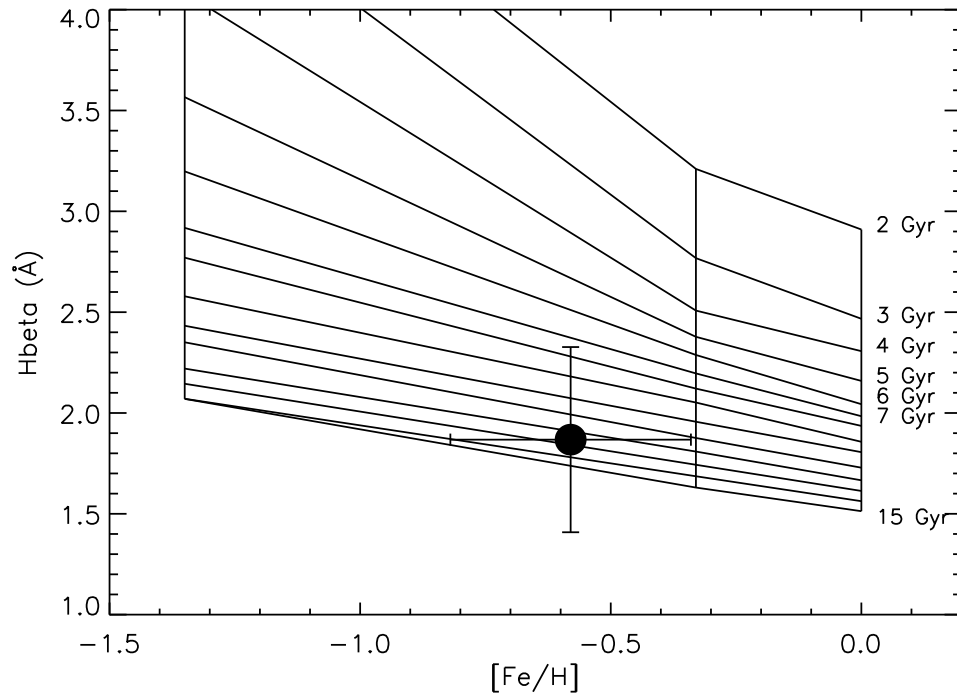


Fig. 8.— $[Fe/H]$ and $H\beta$ estimated from the co-added spectra of objects in NGC 1023 provide a loose constraint on the age of the clusters when compared to the stellar evolutionary models of Maraston & Thomas (2000). The clusters are probably ~ 13 Gyr old but could be as young as ~ 7 – 8 Gyr.

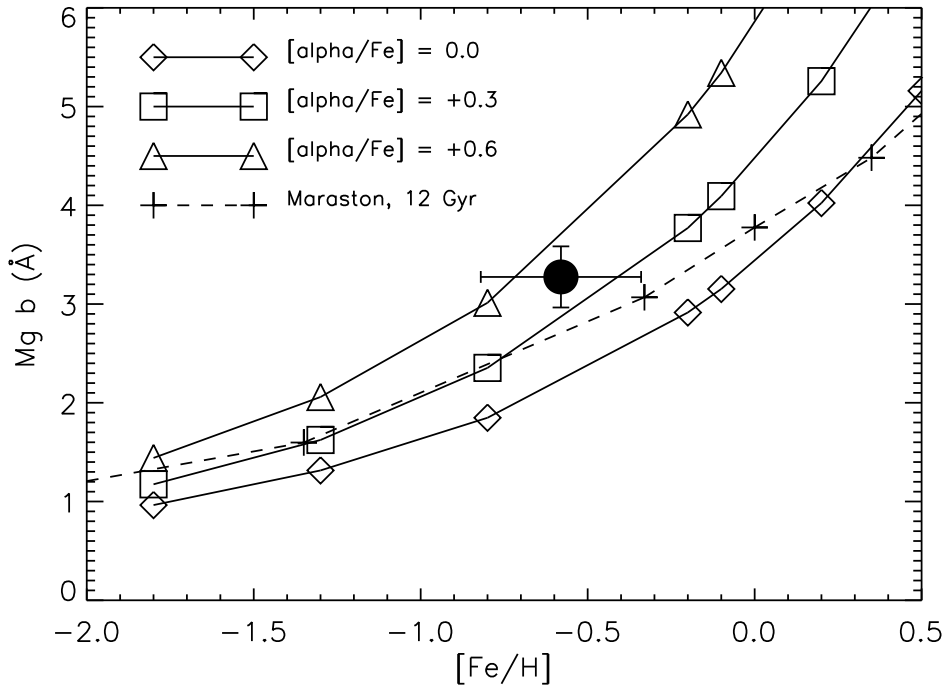


Fig. 9.— $[Fe/H]$ and $Mg\ b$ (solid dot) estimated from the co-added spectra of objects in NGC 1023, compared to SSP model predictions from Milone et al. (2000) for a range of α -element to iron enhancements, assuming a Salpeter IMF. Also shown is the Maraston (2001) SSP curve for a 12 Gyr population.

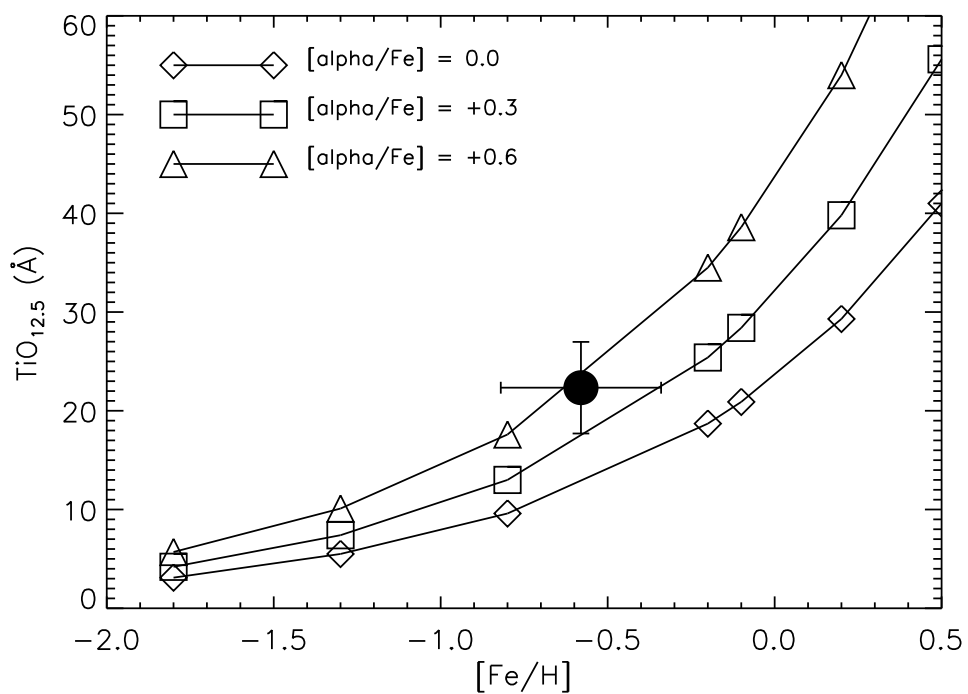


Fig. 10.— $[Fe/H]$ and the $TiO_{12.5}$ index defined in Milone et al. (2000) (solid dot) estimated from the co-added spectra of objects in NGC 1023, compared to SSP model predictions from Milone et al. (2000) for a range of α -element to iron enhancements, assuming a Salpeter IMF.